PCCP

Accepted Manuscript

This is an *Accepted Manuscript*, which has been through the Royal Society of Chemistry peer review process and has been accepted for publication.

Accepted Manuscripts are published online shortly after acceptance, before technical editing, formatting and proof reading. Using this free service, authors can make their results available to the community, in citable form, before we publish the edited article. We will replace this *Accepted Manuscript* with the edited and formatted *Advance Article* as soon as it is available.

You can find more information about *Accepted Manuscripts* in the **Information for Authors**.

Please note that technical editing may introduce minor changes to the text and/or graphics, which may alter content. The journal's standard **Terms & Conditions** and the **Ethical guidelines** still apply. In no event shall the Royal Society of Chemistry be held responsible for any errors or omissions in this *Accepted Manuscript* or any consequences arising from the use of any information it contains.

ROYAL SOCIETY OF CHEMISTRY

www.rsc.org/pccp

Molecular Simulation of Imidazolium-Based Tricyanomethanide Ionic Liquids using an Optimized Classical Force Field

Niki Vergadou[1,], Eleni Androulaki[1,2], Jörg-Rüdiger Hill[3] and Ioannis G. Economou[1,4]*

[1]National Center for Scientific Research "Demokritos", Institute of Nanoscience and Nanotechnology, Molecular Thermodynamics and Modelling of Materials Laboratory, GR-153 10, Aghia Paraskevi Attikis, Greece

[2]University of Crete, Department of Materials Science and Technology, 71003 Heraklion, Crete, Greece,

[3] Scienomics GmbH, Prof.-Messerschmitt-Str. 3, D-85579 Neubiberg, Germany

[4]Texas A&M University at Qatar, Chemical Engineering Program, Education City, PO Box 23874, Doha, Qatar

Corresponding author: n.vergadou@inn.demokritos.gr

1

ABSTRACT   Imidazolium-based ionic liquids (ILs) incorporating the tricyanomethanide ([TCM⁻]) anion are studied using an optimized classical force field. These ILs are very promising candidates for use in a wide range of cutting-edge technologies and, to our knowledge, it is the first time that this IL family is subject to a molecular simulation study with the use of a classical atomistic force field. The [C_4mim^+][TCM⁻] ionic liquid at 298.15 K and at atmospheric pressure was used as the basis for the force field optimization which primarily involved the determination of the [TCM⁻] Lennard-Jones parameters and the implementation of three quantum mechanical schemes for the calculation of the partial charge distribution and the identification of the appropriate scaling factor for the reduction of total ionic charge. The optimized force field was validated by performing simulations of the 1-alkyl-3-methylimidazolium tricyanomethanide ([C_nmim^+][TCM⁻], n = 2, 4, 6, 8) IL family at various temperatures. Results for density, self-diffusivity and viscosity are in very good agreement with the available experimental data for all ILs verifying that the force field reliably reproduces the behaviour of imidazolium-based [TCM⁻] IL family in a wide temperature range. Furthermore, a detailed analysis of the microscopic structure and the complex dynamic behaviour of the ILs under study was performed.

1. Introduction

Ionic liquids (ILs) are salts that are in the liquid state at room temperature and, by convention, below 100 ºC.[1,2]. ILs are characterized by extremely low vapor pressures, wide liquid ranges, non-flammability, good electrolytic and solvation properties and easy recycling. In combination with the aforementioned properties, one of their most important key feature is their chemical tunability that enables the molecular design of task-specific ILs with controlled properties[3,4]. In this direction, molecular simulation significantly contributes in establishing the link between the molecular structure of an IL and its macroscopic properties, providing at the same time a reliable basis for the development of accurate property prediction strategies.

Tricyanomethanide ([TCM⁻]) ILs are identified as very promising in being utilized in a wide range of applications. They exhibit very good thermal and electrochemical stability combined with strong charge delocalization that leads to a weak ion pairing and, hence, to low viscosities and melting temperatures[5, 6]. Imidazolium-based [TCM⁻] ILs, in particular, are considered excellent for use in a number of chemical processes and technological applications such as in gas and aromatic/aliphatic hydrocarbon separations[7], as lubricants of hard coatings and ceramics[8] and as electrolytes in dye-sensitized solar cells[5, 6, 9-11] or in batteries[12]. This IL family has been recently also identified as one of the most attractive IL sorbents for CO_2 capture[13-15] and separation from post-combustion flue gases in state-of-the-art carbon capture technologies.

Computational studies of imidazolium-based [TCM⁻] IL family are limited solely to the study of the 1-ethyl-3-methylimidazolium [TCM⁻] performed by Borodin[16] using an efficient but very complex and computationally expensive many-body polarizable force field. Incorporating polarizability and charge transfer effects has a substantial influence on the computed physical properties[16-21] of ILs. Polarizable force fields permit the response of the ions to the local forces

3

that evolve from the ions of their neighborhood and are therefore more accurate. Nevertheless, taking polarizability explicitly into account entails the implementation of complicated simulation schemes, increasing simultaneously considerably the required computational time.

An alternative approach that has been widely applied in classical molecular simulation studies of ILs[22-31] is the use of reduced partial charges as a simplified effective way to incorporate polarization phenomena and to improve predictions of the dynamic properties that are systematically underestimated in molecular simulations[32, 33] with non-polarizable interaction potentials. Quantum mechanical calculations applied to ILs without any constraints on the total ionic charge resulted also in a sub-integer formal charge[17, 22, 25, 27, 34-37] while charge transfer effects have been detected in experimental studies[38, 39] as well. Recent theoretical studies[40, 41] have focused on unfolding the relation between reduced charges and polarizability effects, investigating the conditions under which a non-polarizable model with scaled charges becomes equivalent to a polarizable one, providing a theoretical basis for charge reduction approach used in IL simulations.

In the present study, imidazolium-based ILs that incorporate the [TCM⁻] anion, namely the [$C_n$mim⁺][TCM⁻] ILs with $n = 2, 4, 6, 8$ being the number of carbon atoms in the alkyl tail, are studied by means of molecular simulation at various temperatures and at atmospheric pressure using an atomistic classical force field. The [C_4mim⁺][TCM⁻] IL was used as test system for the force field optimization procedure that took place at 298.15 K, having as an ultimate target the accurate prediction of the [C_4mim⁺][TCM⁻] density and the cation's self-diffusion coefficient. The optimization mainly focused on the determination of the [TCM⁻] Lennard-Jones (LJ) parameters and the identification of the scaling factor for the total ionic charge. For the latter, partial charges were calculated quantum mechanically using three different schemes based: (a)

on the isolated ions, (b) on four minimum energy conformations of the ion pair and (c) on two

ion pairs of $[C_4mim^+][TCM^-]$ in order to meaningfully estimate the scaling factor of the atomic

charge distribution to be used in the proposed force field. The final optimized force field was

validated at higher temperatures and in $[C_nmim^+][TCM^-]$ ILs (with $n = 2$, 6, 8) of the same

family varying the alkyl tail length of the cation.

Results on density and transport properties, namely self-diffusivities and viscosities, are in very

good agreement with experimental data revealing the ability of the force field in use to reliably

reproduce the behavior of the imidazolium-based $[TCM^-]$ IL family in a wide temperature range.

Structural properties were calculated for all systems under study and further insight into the

characteristics of the ILs dynamics was obtained by analyzing the anisotropy in the ions

translational motion. Dynamic heterogeneity phenomena were quantified[42] and ions that move

faster or slower than expected were detected to be highly spatially correlated. The alkyl tail

length and the temperature dependence of the above properties was examined.

2. Force field

The all-atom force field used to describe the potential energy of the molecular systems is

given by the following expression:

$$
\begin{aligned}
U = \sum_{bonds} k_b \, (b - b_0)^2 + \sum_{angles} k_\theta \, (\theta - \theta_0)^2 + \sum_{dihedrals} \sum_{n=1}^{4} k_\chi [1 + cos(n\chi - \delta)] \\
+ \sum_{impropers} k_\psi \, (\psi - \psi_0)^2 + \sum_{\iota=1}^{n-1} \sum_{j>1}^{n} \left\{ \left[\left(\frac{\sigma_{ij}}{r_{ij}} \right)^{12} - \left(\frac{\sigma_{ij}}{r_{ij}} \right)^6 \right] + \frac{q_i q_i}{4\pi\varepsilon_0 r_{ij}} \right\}
\end{aligned}
\tag{1}
$$

where b, θ, χ and ψ denote bond length, bond angle, dihedral and improper angle, respectively, and the subscript "0" refers to the equilibrium values. Parameter n in the term of the dihedral potential is the multiplicity of the dihedral angle while δ is the phase shift of the dihedral potential over the full range of rotation. Partial charges are denoted by q_i, ε_0 is the vacuum permittivity and ε, σ the Lennard-Jones (LJ) parameters.

2.1. Quantum Mechanical Calculation of Charges

One of the major problems with force fields for ILs that is still under debate[20, 21, 43-45] is the estimation of charges. The correct prediction of intermolecular interactions within a force field requires a delicate balance between attractive (electrostatic) and repulsive (van der Waals) forces. Charges can in principle be calculated using quantum mechanical methods. Since charges are not quantum mechanical observables, the assignment of electron density to each atom in a moiety is to some degree arbitrary. A common practice is to use charges that reproduce the electrostatic potential of a chemical compound[46] and this approach was followed in the present study. Charge calculations were performed using three schemes in order to study the effect of the system size on the charge distribution obtained. First, we used isolated ions. Subsequently, an anion-cation pair was considered. In this case, the relative configuration of the cation and the anion is to be determined and therefore, calculations had to be carried out for a number of different conformations. Finally, the charge distribution was also calculated using a cluster of two ion pairs.

Quantum chemical calculations of charges for ILs are often carried out using density functional theory (DFT)[21]. However, these methods are problematic for a number of reasons. The

choice of the functional is not straightforward. It has been shown that hybrid functionals such as

B3-LYP[47] which normally perform quite well for organic molecules do not give results as

good[43,37,48] as simpler functionals such as PBE[49]. Furthermore, DFT does not account for

dispersion interactions which are of importance for the structure of ILs and can give unphysical

charge transfer[21]. Finally, a systematic improvement of the predictions of the DFT calculations is

not possible. Due to these limitations, we used Møller-Plesset perturbation theory (MP2) as a

post-Hartree-Fock method for the calculation of charges in accordance with other developments

of force fields for ILs[50]. Comparisons with more elaborate electronic structure methods indicate

that MP2 is trustworthy in this respect[21]. Its implementation with the resolution of identity

approach (RI-MP2[51,52]) is fast enough to allow the treatment of ions of the size needed for this

study. In all cases, the structure of the ions was optimized using the RI-MP2 method with a 6-

311++G** basis set[53] and a def-SV(P) basis set[54] as auxiliary basis set.

2.1.1. Charges from isolated ions

In the calculations of isolated ions, a total ionic charge of +1e or -1e was assigned to cations

and anions, respectively. In Tables S1 and S2 of the Supplementary Information the charges

obtained for the imidazolium cations and the [TCM$^-$] anion, respectively, are shown. There is a

lot of similarity in the charge distributions of the different cations. In all cases, the largest partial

atomic charges can be found at the carbon atoms of the methyl groups at both ends of the

molecule, the carbon atoms in the imidazolium ring have almost no charge and the two nitrogen

atoms are equivalent with respect to the charges. In total, about half of the ionic charge is located

in the imidazolium ring, while the negative charge is smeared over the entire anion.

2.1.2. Charges from one ion pair

For $[C_4mim^+][TCM^-]$ a series of different conformations of ion pairs were studied. Four different minimum energy conformations were used. Table 1 shows the conformers of $[C_4mim^+][TCM^-]$ and their relative energies. The relative orientation of cation and anion is almost the same in all cases. The imidazolium ring and the anion are located in parallel planes with a distance of about 3 Å. The four conformations are all very close energetically and the energy differences are within the range of thermal energy even at room temperature. Therefore, it can be expected that all these conformations will be present in an ionic liquid at room temperature. The conformational flexibility is mostly dominated by changes in the torsion angles of the butyl group.

The differences of the charges obtained for the different conformations are small. Tables S2 and S3 list the average charge for each atom (and the standard deviation) in comparison with the charges obtained for the isolated ions. In the calculation of the partial charges for the isolated ions, a charge of ±1e was imposed on the ions while in the calculations for the ion pairs the system was allowed to distribute the charge between cation and anion without imposing any constrains. The total ionic charge in this case is significantly lower. This agrees with findings by previous computational studies and experiment[21]. The total ionic charge over the four minimum energy configurations ranges from ±0.716e to ±0.756e, with a mean value of ±0.7355e. Consequently, the partial charges are also lower in this case. With a few exceptions, the charges obtained for the different conformations of the ions pairs are similar as can be seen from the low standard deviations. The largest deviations appear for the carbon atoms in the butyl group and are probably related to the different torsion angles in the different conformations.

8

2.1.3. Charges from a small cluster of ions

In order to verify the charges obtained for ion pairs, an MP2 calculation has been performed on a small cluster consisting of two cations and two anions. The system was fully optimized and then the charges were calculated by fitting the electrostatic potential. Figure 1 shows a representative structure of $[C_4mim^+][TCM^-]$ ion cluster obtained by geometry optimization along with the calculated charges.

Although the ion pairs show a more or less stacked structure of the cation and the anion, the orientation of the anions is different in the cluster. One of the anions remains parallel to the imidazolium ring of the cation, but the second one takes a position more or less perpendicular to the imidazolium plane. The second cation is again oriented almost parallel to the second anion. There is no significant difference between the charges for the two cations. The charges on the anions vary depending on the position of each anion in relation the other three ions of the cluster. Namely, the charges on the anion on the left which interacts only with one cation are larger than the charges for the second anion which interacts with both cations. In particular, the charge on the central carbon atom changes from -0.50e to -0.33e. Since $[TCM^-]$ possesses π electrons which are delocalized over the entire ion, the anion charge distribution is apparently able to adapt very easily to changes in the environment. The total charge of each ion also varies significantly. The total charge of the $[C_4mim^+]$ cation in the middle between the two $[TCM^-]$ anions is 0.769e while it is 0.651e for the other $[C_4mim^+]$ ion. The total charges of the $[TCM^-]$ anions are -0.828e and -0.592e and are more diverse than the ones for the cations. The mean total ionic charge obtained from the calculation on the small cluster is equal to ±0.71e, slightly lower than the one

calculated for the ion pair (±0.7355e) , indicating that it is meaningful for the IL under study to be represented by a reduced total ionic charge of the order of ±0.70 - 0.75e.

2.2. Force Field Optimization

The [C$_4$mim$^+$][TCM$^-$] IL was chosen as a benchmark system and all the simulations at this stage were performed at 298.15 K and at atmospheric pressure. The force field optimization procedure focused on (*i*) the study of the effect of the charge distribution on the calculated properties, (*ii*) the appropriate choice of the charges scaling factor to effectively incorporate polarizability and charge transfer effects and, at the same time, (*iii*) the determination of the [TCM$^-$] anion LJ parameters in order to attain good agreement with the experimental data for both the density and the self-diffusivity. The experimental data for the density of [C$_4$mim$^+$][TCM$^-$] used for comparison were taken from Ref. [13], whereas the experimental measurement of the [C$_4$mim$^+$] cation's self-diffusion coefficient was performed[55] at the Institute of Chemical Reaction Engineering of the University of Erlangen-Nuremberg, Germany following the procedure that is described in Ref. [56]. Two different charge distributions have been tested: partial charges as calculated on isolated ions (abbreviated ISO) and as determined from the mean total ionic charge obtained by the four minimum relative energy conformations of the ionic pair (abbreviated 4RC). In both charge distributions, necessary modifications were performed in the anion's charges so that atoms in symmetrical positions have the same charge.

The cations' bonded and LJ parameters were obtained from Cadena and Maginn[57]. Bonded and LJ parameters for the [TCM$^-$] anion were available only for the case of a [TCM$^-$] IL coupled to 1-ethyl-1-methylpholinium cation. These were taken from a technical report by Martin *et al.*[58] Using directly the anion's LJ parameters of Martin *et al.*[58] and the above mentioned charge

distributions for the molecular simulation of $[C_4mim^+][TCM^-]$ at 298 K results in a significant underestimation of the diffusivity which is calculated in the range of $10^{-8} - 10^{-9}$ cm^2/s. Although this diffusivity range is too slow to be accurately sampled by MD, we indicatively mention that use of 4RC partial charge distribution with this initial set of parameters resulted in a cation's self-diffusion coefficient almost one and a half orders of magnitude lower than the experimental one. With the same set of parameters the diffusivity predictions with the ISO scheme, was two orders of magnitude lower when scaled to 0.80e and more than one order of magnitude lower with a scaling to 0.75e, indicating that apart from the total ionic charge itself, the distribution of partial charges also influences the calculated diffusivity.

The optimization procedure was implemented through systematic modification of the anion's LJ parameters using both partial charge schemes and probing various scaling factors for the total ionic charge. For each set of parameters, long molecular dynamics (MD) simulations were performed as described in Section 3.1, with the primary target being the prediction of density within 1% deviation from experimental data and, subsequently, the calculation of the diffusion coefficient. From these test simulations it was observed that in order to obtain an equally good agreement on the self-diffusivities from the two charge schemes, the 4RC charge distribution needed to be reduced to a slightly lower total ion charge compared to ISO scheme.

In the analysis that follows, the ISO scheme was chosen to be used due to the fact that it retains a degree of transferability in the proposed force field compared to the 4RC scheme, with the latter requiring individual and more elaborate quantum mechanical computations for each IL pair of the imidazolium-based TCM family under study. The ISO set of parameters scaled to ±0.75e total ionic charge was identified as being the optimum one to realistically represent the ionic liquid systems at hand, resulting in a deviation of less than 0.1% from experimental density

11

and less than 5% in the calculated self-diffusivity at 298.15 K. The set of parameters of the optimized force field to be used with the ISO charge scheme scaled to ±0.75e are given in the Supporting Information (Tables S4 and S5).

3. Simulation Details

The proposed force field that was optimized for the case of $[C_4mim^+][TCM^-]$ at 298.15 K was validated against experimental data by performing MD simulations at various temperatures. At the same time, the transferability of the new parameters for $[TCM^-]$ when paired with other imidazolium-based cations varying the cation alkyl chain length was also studied. For this, simulations of four ILs, namely, $[C_2mim^+][TCM^-]$, $[C_4mim^+][TCM^-]$, $[C_6mim^+][TCM^-]$ and $[C_8mim^+][TCM^-]$, were performed at three temperatures (298.15 K, 363.14 K and 398.15 K), and at atmospheric pressure. Bonded and LJ parameters $[C_nmim^+]$ cations are obtained with some slight modifications from the literature[57, 59, 60] and are given in the Supporting Information (Tables S5-S6).

Long MD simulations of 200 $[C_nmim^+][TCM^-]$ ($n = 2, 4, 6, 8$) ion pairs were performed using the software code NAMD[61] using four independent initial configurations for each IL system at each temperature. The initial structures were built using the Rotational Isomeric State (RIS) model[62] as modified by Theodorou and Suter[63,64] available in MAPS[65]. The ions were placed in the simulation box at the experimental density, if available, or at the value calculated by extrapolating the available experimental data. A conjugate gradient energy minimization procedure of 10^5 steps was applied to eliminate the atomic overlaps, followed by a short simulation of 5 ns in the canonical ensemble (NVT). Afterwards, a 25 ns simulation in the isobaric-isothermal ensemble (NPT) was performed in order to relax the system and calculate the

density. Subsequently, simulations of 20 ns were performed in the canonical ensemble (NVT) at

the mean density, as obtained from the NPT simulations. Finally, simulation runs of the order of

30ns were conducted in the microcanonical ensemble (NVE) to calculate the transport properties.

Control of the temperature was performed using a Langevin piston with a 5 ps^{-1} damping

factor while the Nosé-Hoover barostat was used for pressure control with an oscillation period

equal to 200 fs and a damping factor of 100 fs. Electrostatic interactions were handled by means

of the particle-mesh Ewald method[65], while the electrostatic interactions between atoms

connected with three bonds were scaled by a factor of 0.5. The reversible reference system

propagator algorithm (rRESPA[66,67]) was used as a multiple time step algorithm in order to speed

up the MD simulations. The reference time step was 1 fs for the NVT and NPT simulations and

0.5 fs for the NVE ensemble. Short-range non-bonded van der Waals interactions were

calculated every 2 fs and the full electrostatic interactions were computed every 4 fs in the NVT

and NPT runs and in case of NVE simulations these were calculated every 1 fs and 2 fs,

respectively. A cutoff distance of 12 Å was used to truncate the van der Waals interactions using

a switching function beyond 10.5 Å. A long-range correction was applied to the system's energy

and virial to account for the neglected van der Waals forces due to switching and cutoff of the

Lennard-Jones potential. The Lorentz-Berthelot mixing rules were used to calculate the force

field parameters between unlike atoms.

4. Results and Discussion

4.1 Density and transport properties

MD simulation results for density of the four ILs at various temperatures are shown in

Figure 2, together with experimental data[13,15,68,69,70,71] for $[C_n mim^+][TCM^-]$, n=2,4,8 ILs. No

experimental data were found in the literature for [C$_6$mim$^+$][TCM$^-$] IL. The maximum deviation

between experimental data and MD simulations is 1.2 % for [C$_2$mim$^+$][TCM$^-$], 0.7 % for

[C$_4$mim$^+$][TCM$^-$] and 1.2 % for [C$_8$mim$^+$][TCM$^-$]. Mean density values from MD are provided in

Table 2.

Calculation of the ions self-diffusion coefficients was performed using the Einstein relationship:

$$D = \frac{1}{6} \lim_{t \to \infty} \frac{d}{dt} \langle |\mathbf{r}_i(t) - \mathbf{r}_i(0)|^2 \rangle \tag{2}$$

where $\mathbf{r}_i(t)$ is the position of the i-th ion's center of mass at time t and the brackets denote the

mean-square displacement (MSD) over all ions' centers of mass. The diffusion coefficients were

calculated in the Fickian regime, which is identified by a slope equal to unity in the log(MSD)

versus log(t) plot.

In Figure 3 the calculated diffusivities for the four ILs at all temperatures are plotted as a

function of the number of the carbon atoms in the cation's alkyl tail. Experimental NMR

measurements[55, 72] for the cations diffusivity at 298.15 K for [C$_n$mim$^+$][TCM$^-$], (n=2,4,8), as

well as at 398K for [C$_8$mim$^+$][TCM$^-$] are also plotted for comparison and appear to be in good

agreement with the predicted values. The predicted diffusion coefficient for [C$_2$mim$^+$] cation is

also in very good agreement with the calculated value from Borodin[16] obtained with the use a

many-body polarizable force field (star symbol in Fig.3). It is obvious in Figure 3 that as the

alkyl tail becomes longer the ions diffusivity decreases. For the case of smaller (and lighter)

cations e.g. [C$_2$mim$^+$] (mass 111.1645 amu) that has a mass comparable to one of the [TCM$^-$]

anion (90.0629 amu), the self-diffusion coefficients of the two counterions are rather similar. As

the cation's alkyl tail becomes longer, and thus the cation becomes heavier (mass of

[C$_8$mim$^+$] = 195.3235 amu), the anion's self-diffusion coefficient becomes higher. No

experimental data on anions diffusivity are currently available. MD predictions for the self-

diffusivities are also provided in Table 3. Diffusivity results of [C$_8$mim$^+$][TCM$^-$] in the temperature range 298 K - 398 K are plotted against experimental data in Figure 4. Agreement between experiments and simulations is very good in all cases.

Shear viscosity calculations were performed using the Green-Kubo relationship:

$$\eta = \frac{V}{k_B T} \int_0^\infty dt \langle P_{ij}(t) P_{ij}(0) \rangle \tag{3}$$

where $P_{ij}(t)$ is the ij-element of the pressure tensor at time t ($i \neq j$). The pressure tensor was stored every 8 fs at the last section of each productive NVT run and the viscosity was estimated by the integral plateau value at a region in which the pressure autocorrelation function was fluctuating around zero. In Figures 5a-d the viscosities of [C$_2$mim$^+$][TCM$^-$], [C$_4$mim$^+$][TCM$^-$], [C$_6$mim$^+$][TCM$^-$] and [C$_8$mim$^+$][TCM$^-$], respectively, are plotted as a function of temperature and are compared to experimental data[13,15,69,71,73]. The agreement between the experimental data and the predicted values is good with the temperature dependence of the viscosity being captured very well taking into account the fact that viscosity is a collective property and, thus, difficult to be reproduced. In the case of [C$_2$mim$^+$][TCM$^-$], there is an overestimation by the predicted values in accordance with the slightly lower values of the calculated cation self-diffusivities.

4.2 Structure properties

Radial distribution functions (RDFs) between the centers of mass of the ions and between various atoms of the ions have been calculated in order to study the microscopic structure of the ILs. In Figure 6, the RDFs between the centers of mass for anion-anion, anion-cation and cation-cation interactions are shown for (a) [C$_2$mim$^+$][TCM$^-$], (b) [C$_4$mim$^+$][TCM$^-$], (b) [C$_6$mim$^+$][TCM$^-$] and (c) [C$_8$mim$^+$][TCM$^-$] at 298.15 K. Due to the strong interaction between ions carrying opposite charges, the highest maximum is observed for the anion-cation RDF and it

appears at a distance of 5 Å in all cases. The anion-anion RDF has two maxima: a small one at around 4 Å and a higher at 9 Å. This is unlike the anion-anion RDF calculated for $[C_n mim^+][Tf_2N^-]$ ILs[25] that exhibits only one maximum at around 9 Å. The existence of the smaller maximum at short distance is attributed to the smaller size of the $[TCM^-]$ anion and the weaker ion pairing that allows a more uniform anion distribution around the cations than the bulkier $[Tf_2N^-]$ anion. Going from smaller to longer alkyl tails, the peak of the anion-cation RDF (red line in Figure 6) increases from $[C_2 mim^+][TCM^-]$ to $[C_4 mim^+][TCM^-]$ and $[C_6 mim^+][TCM^-]$ and becomes sharper while it decreases in $[C_8 mim^+][TCM^-]$ again becoming simultaneously broader. At the same time, the peak of RDF that corresponds to the cation-cation interaction (green line) also decreases as the alkyl tail becomes longer. This behaviour can be attributed to the shift of the location of the cation's center of mass due to the varying size and flexibility of the alkyl tail.

More information on the microscopic structure can be obtained from RDFs between specific atoms on the ions. In Figure 7, the RDFs between the terminal carbon atoms of the cation's alkyl tail are plotted for the four ILs at 298.15 K. In all cases, there is one maximum at around 4 Å that becomes more intense as the alkyl tail becomes longer, thus indicating the existence of tail aggregation phenomena. This is in accordance with previous simulation studies[25,74,75,76,77] of imidazolium-based ILs and is attributed[77] to the almost neutral charge of the alkyl tail that results in stronger short-ranged van der Waals interactions which lead to the formation of non-polar domains. At the same time, as the alky tail becomes longer the anion is found to be more strongly correlated with the charged imidazolium ring as shown in Figure 8 where the RDFs between the C2 carbon which is located on the most charged part of the imidazolium ring, and the negatively charged nitrogen NC of the anion are plotted for all ILs at 298.15 K. The first

intense maximum appears at around 3 Å, whereas there are two small peaks at longer distances which correspond to the other two, same-type nitrogens NC. The fact that the [TCM⁻] anion is more strongly correlated with the charged part of the cation for the cases of longer alkyl tails is also supported by the fact that for the longer alkyl tail the [TCM⁻] is found to be less associated with the terminal part of the almost neutral alkyl tail (see Figure S3).

4.3 Analysis of the dynamical behavior

a. Anisotropy in the cation's translational motion

The translational motion of the center of mass of cations was analyzed along various axes specified by the geometry of the cation. In particular, the displacement of a center of mass during a time interval $t - t_0$ was projected onto the following axes at time t_0: the vector NN that connects the two nitrogen atoms in the imidazolium ring, the normal vector to the imidazolium ring, the vector NNp that is perpendicular to the former two vectors and the end-to-end vector N3-Ct of the alkyl tail (see Figure S4). In Figure S5, the MSDs along these axes are plotted against the 1/3 of the total MSD for the four ILs at 298.15 K. For the [C_2mim⁺] cation that has the shortest alky tail, MSD calculations along the various vectors are close to each other. However, there is a slightly enhanced movement along the NN vector, a fact that becomes more pronounced as the alkyl tail becomes longer. In the case of [C_8mim⁺] at 298 K, the MSD along N3-Ct is almost 50% higher than the 1/3 of the total MSD at 1.5 ns. These findings are in accordance with similar analysis performed for imidazolium-based ILs that incorporate the [Tf$_2$N⁻] anion[78] and also with the results of Liu and Maginn[24] on [C_4mim⁺][Tf$_2$N⁻]. This anisotropy in the cations translational motion is preserved over long timescales that reach even in the Fickian regime at 298.15 K.

b. Cluster formation of dynamically distinguishable ions

The heterogeneity in the dynamics can be quantified by the calculation of the non-Gaussian parameter $a_2(t)$ given by the formula[42]:

$$a_2(t) = \frac{3\langle |\boldsymbol{r}_i(t) - \boldsymbol{r}_i(t_0)|^4 \rangle}{5\langle |\boldsymbol{r}_i(t) - \boldsymbol{r}_i(t_0)|^2 \rangle^2} - 1 \tag{4}$$

where $|\boldsymbol{r}_i(t) - \boldsymbol{r}_i(t_0)|$ is the displacement of an ion's center of mass at the time interval $t - t_0$. In case of a Gaussian distribution of $|\boldsymbol{r}_i(t) - \boldsymbol{r}_i(t_0)|$, $a_2(t)$ is zero while any deviations from zero indicate the presence of heterogeneities in the dynamics. In Figure S6(a-d), $a_2(t)$ for [C_2mim$^+$][TCM$^-$], n=2,4,6,8 is shown as calculated at 298.15 K. Dynamic heterogeneity is present in all IL systems, and $a_2(t)$ is higher at all cases for the anion and for the longer alkyl tails while it is also preserved at longer time scales. As the temperature increases, $a_2(t)$ reaches zero faster whereas its maximum is less intense and is observed earlier (not shown here).

The presence of dynamically distinguishable ions is quantified by the deviation of the self-part of the van Hove function $G_s(\mathbf{r}, t)$ from the expected Gaussian distribution. The $G_s(\mathbf{r}, t)$ is the probability that a particle is at position $\mathbf{r}_i(t)$ at time t given that it was located at $\mathbf{r}_i(0)$ at time 0 and is given by the formula[79]:

$$G_s(\mathbf{r}, t) = \frac{1}{N} \langle \sum_{i=1}^{N} \delta[\mathbf{r} + \mathbf{r}_i(0) - \mathbf{r}_i(t)] \rangle = \frac{1}{N} \langle \sum_{i=1}^{N} \delta[\Delta \mathbf{r}(t)] \rangle \tag{5}$$

From the deviations of $G_s(\mathbf{r}, t)$ from the Gaussian distribution at short and long

18

distances one can identify ions that have moved less or more than expected at a specific time interval[80]. This phenomenon is depicted by an intersection of the self-part of the van Hove function $G_s(\mathbf{r}, t)$ with the expected Gaussian distribution when plotted in a comparative manner as shown in Figure 9 for the [C$_4$mim$^+$][TCM$^-$] ions at 298.15 K and at various time intervals. The intersection of the two curves at short distances (r_1) and long distances (r_2) is indicative of ions with low and high mobility, respectively, according to the distance that each ion has travelled at time t. More details on the procedure used for these calculations are presented in Ref.[78]. RDFs between ions that are found to move faster and slower than expected have been calculated in order to investigate the correlation of these ions in space. In Figure 10, RDFs between dynamically distinguishable anions and cations of [C$_4$mim$^+$][TCM$^-$] at 298.15 K are plotted against the total $g(r)$ as calculated without any discrimination on the dynamic behaviour of the ions. The maxima of all the RDFs appear at the same distances, however, the RDFs between fast anions – fast cations and slow anions – slow cations exhibit a much higher peak compared to the total RDF whereas, on the other hand, the RDF between fast and slow ions has a much lower peak. Similar observations have been made for all ILs under study and for the cation-cation and anion-anion RDFs as well. These findings indicate the formation of clusters in the bulk that are comprised of dynamically distinguishable ions.

4. Conclusions

A classical atomistic force field was proposed for imidazolium-based tricyanomethanide ([TCM$^-$]) ILs. The optimization of the force field was performed on

the basis for accurate prediction of the density and the cation self-diffusion coefficient of [C$_4$mim$^+$][TCM$^-$] at 298.15 K by tuning the Lennard-Jones parameters of the anion and simultaneously testing various charge distributions. The charge distribution obtained from quantum mechanical calculations on isolated ions was finally chosen as it is transferable, compared to charge distributions calculated on four minimum energy configurations of the ion pair. Polarizability and charge transfer effects are incorporated in a simplified effective way into the system by uniformly scaling the atomic charges to yield an ionic total charge of ±0.75e, as dictated by the reduced ionic charge determined in the quantum mechanical study on an ion pair and on a small ion cluster.

The accuracy of the optimized force field was tested at higher temperatures, namely 363.15 K and 398.15 K, and for ILs consisting of cations with shorter and longer alkyl tails. The agreement between measured and predicted densities and transport properties of all ILs under study confirms the efficiency of the proposed force field for imidazolium-based [TCM$^-$] ILs. The force field captures well the temperature dependence of the density, diffusivity and viscosity and the prediction for [C$_2$mim$^+$] cation self-diffusivity is very close to the one obtained with the use of a complex polarizable force field.

Detailed study of the structural properties of the ILs revealed a trend for aggregation of the cation's alkyl tail that is more pronounced for the longer ones while the anion was found to be more preferably situated near the imidazolium ring. Further analysis on the ions translational motion revealed anisotropy in the cations translational motion with an enhanced movement along the vector that connects the two nitrogen atoms in
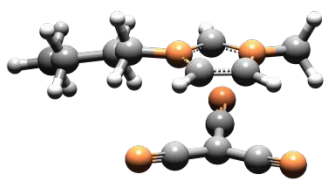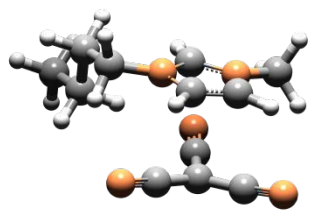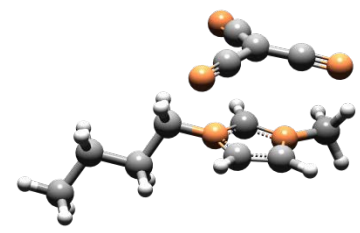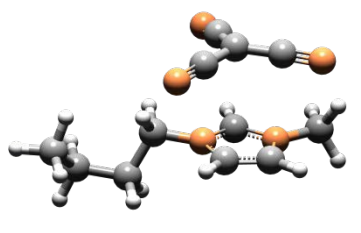
the imidazolium ring and along the end-to-end vector of the alkyl tail. The heterogeneity in the dynamics of the ILs under study is investigated through the calculation of the non-Gaussian parameter and dynamically distinguishable ions are detected and found to be highly spatially correlated.

The predictive ability of the validated force field constitutes a reliable starting point for the study of a wide range of properties of the imidazolium-based [TCM⁻] family, such as simulation of confinement effects and calculation of gas permeability and selectivity properties that are currently underway.

Acknowledgements

Table 1: The conformers of [C$_4$mim$^+$][TCM$^-$] and their relative energies as calculated from RI-MP2 method on one ion pair.

Structures and Relative MP2 energy	
0.0 (kJ/mol)	**2.0 (kJ/mol)**
4.7 (kJ/mol)	**5.1 (kJ/mol)**

Table 2: Mean mass density values for the four ILs at different temperatures and 1 bar using four individual configurations for each IL at each temperature.

T (K)	Mass Density (gr/cm^3)			
	$[C_2mim^+][TCM^-]$	$[C_4mim^+][TCM^-]$	$[C_6mim^+][TCM^-]$	$[C_8mim^+][TCM^-]$
298.15	1.0943±0.0002	1.0483±0.0006	1.0237±0.0004	0.9967±0.0003
363.15	1.0409±0.0001	0.9968±0.0001	0.9742±0.0002	0.9480±0.0003
398.15	1.0126±0.0001	0.9699±0.0001	0.9480±0.0002	0.9228±0.0003

Table 3: Mean self-diffusion coefficients of the ions' center of mass for the four ILs at different temperatures and at 1 bar using four individual configurations for each IL at each temperature.

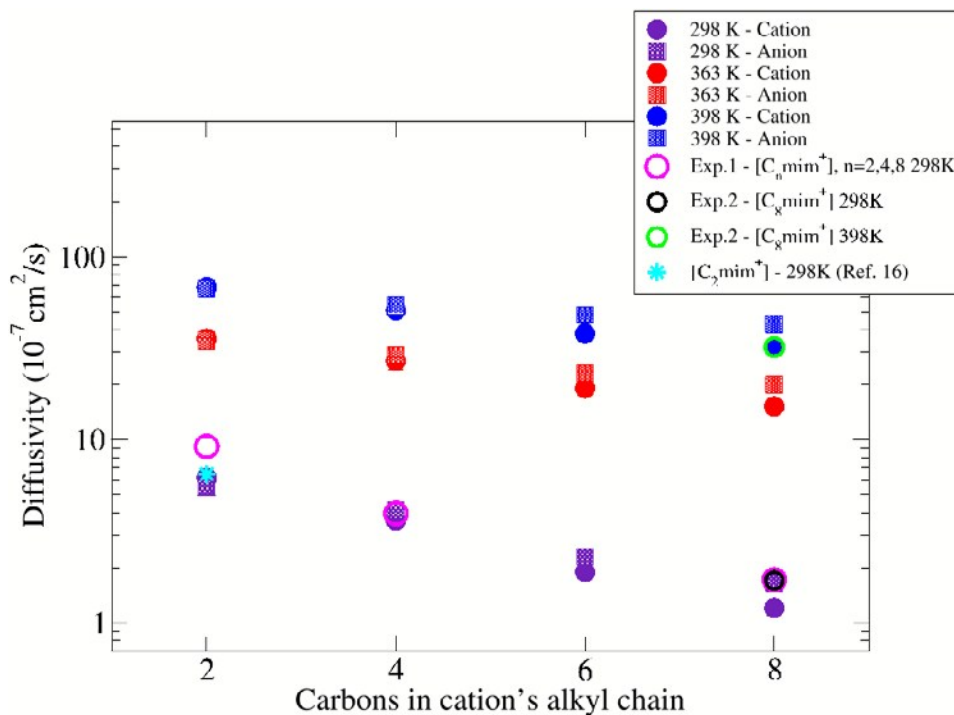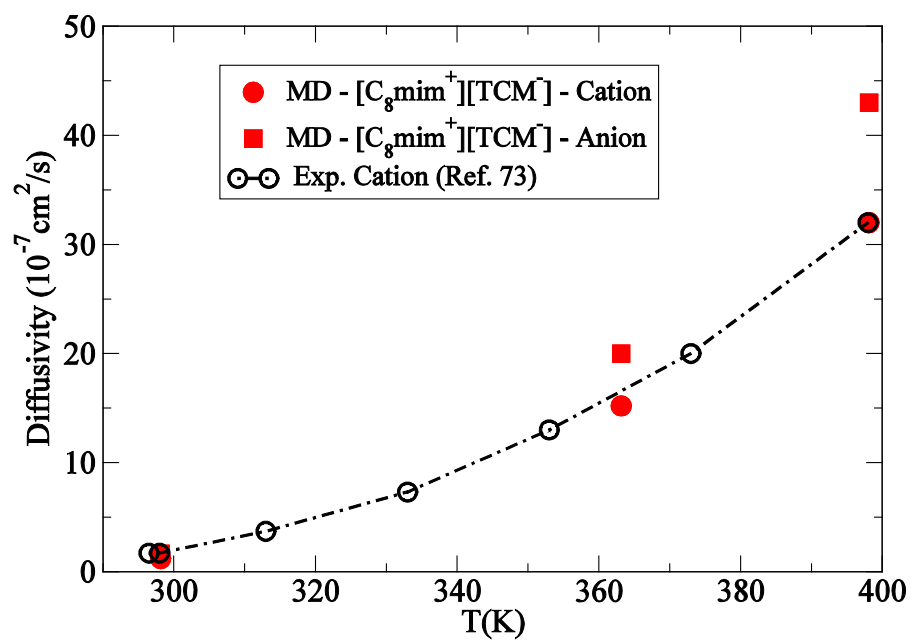| T (K)	Self Diffusion Coefficients (10^{-7}cm^2/s)							
	$[C_2mim^+][TCM^-]$		$[C_4mim^+][TCM^-]$		$[C_6mim^+][TCM^-]$		$[C_8mim^+][TCM^-]$	
	Anion	Cation	Anion	Cation	Anion	Cation	Anion	Cation
298.15	5.4±0.2	6.2±0.6	4.1±0.4	3.6±0.4	2.4±0.2	1.9±0.1	1.64±0.04	1.2±0.1
363.15	35±1	35.7±0.8	29±1	27±3	23.1±0.9	19.1±0.5	20.0±0.7	15.2±0.8
398.15	67±1	68±3	54±3	51±1	48±2	38±2	43±1	31.7±0.7
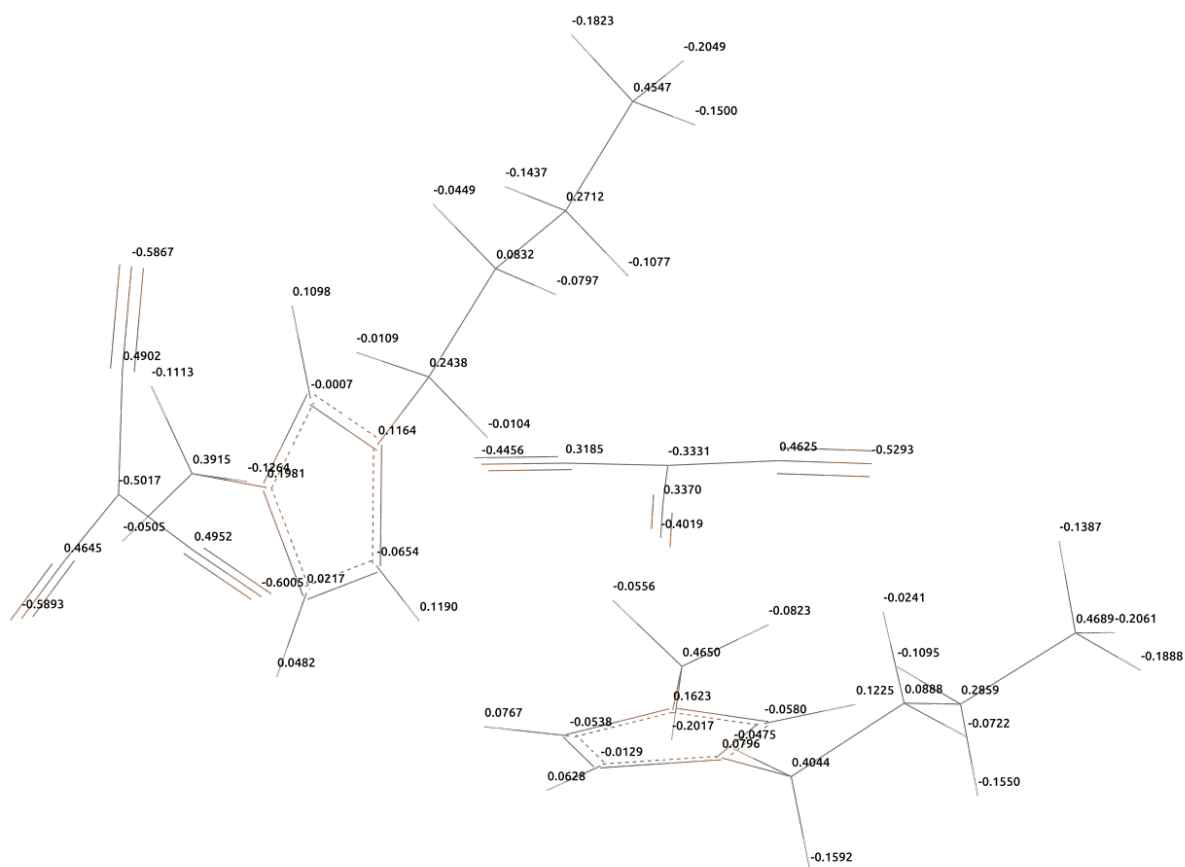
**Figure 1:** The structure of two pairs of [C$_4$mim$^+$][TCM$^-$] with charges obtained from the quantum mechanical calculations.
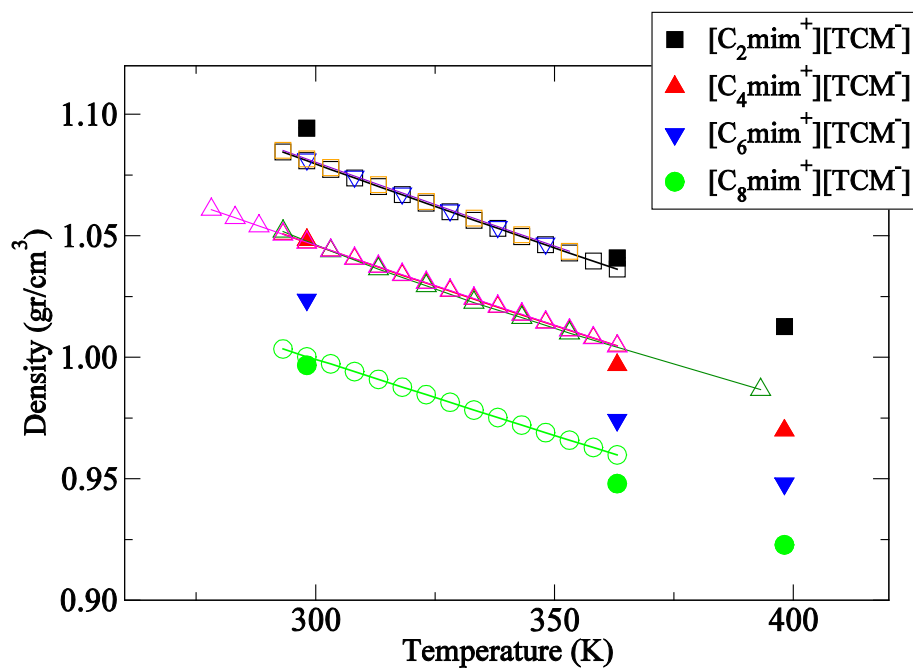
Figure 2: Mean density of [C$_n$mim$^+$][TCM$^-$], n = 2, 4, 6, 8. MD predictions (full points) and experimental data (open points) for [C$_2$mim$^+$][TCM$^-$][13,68,69], [C$_4$mim$^+$][TCM$^-$][13,70,71] and [C$_8$mim$^+$][TCM$^-$].[15] Lines are fit to the experimental data. The error bars in the MD predictions are within the symbol size.

Figure 3: Self-diffusion coefficients (as calculated from four independent simulation runs) of the anion (circles) and the cation (squares) versus the carbon atoms in the cation alkyl tail as calculated at 298.15 K (black), 363.15 K (red) and 398.15 (blue). The open circles are the experimental measurements[55, 72] of the cation diffusivity at 298.15 K and the star symbol corresponds to a molecular simulation prediction[16] using a polarizable force field. The error bars in the MD predictions are within the symbol size.

Figure 4: Self-diffusion coefficients of the anion (circles) and the cation (squares) versus temperature for [C$_8$mim$^+$][TCM$^-$]. The open points correspond to experimental results[72]. The error bars in the MD predictions are within the symbol size.
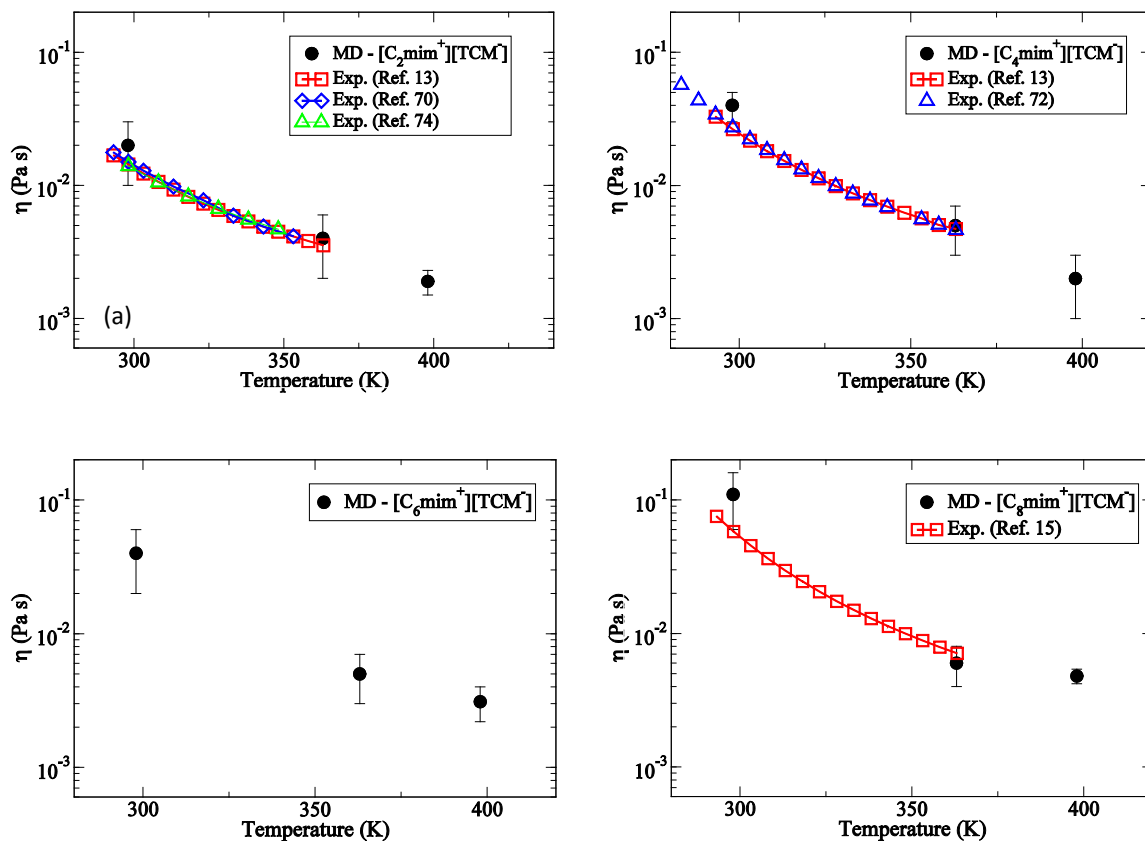
Figure 5: Viscosity calculations from four independent MD simulations (full points) as a function of temperature against experimental data (lines with open points) when available for (a) [C₂mim⁺][TCM⁻]¹³,⁶⁹,⁷³, (b) [C₄mim⁺][TCM⁻]¹³,⁷¹ , (c) [C₆mim⁺][TCM⁻]and (d) [C₈mim⁺][TCM⁻]¹⁵.
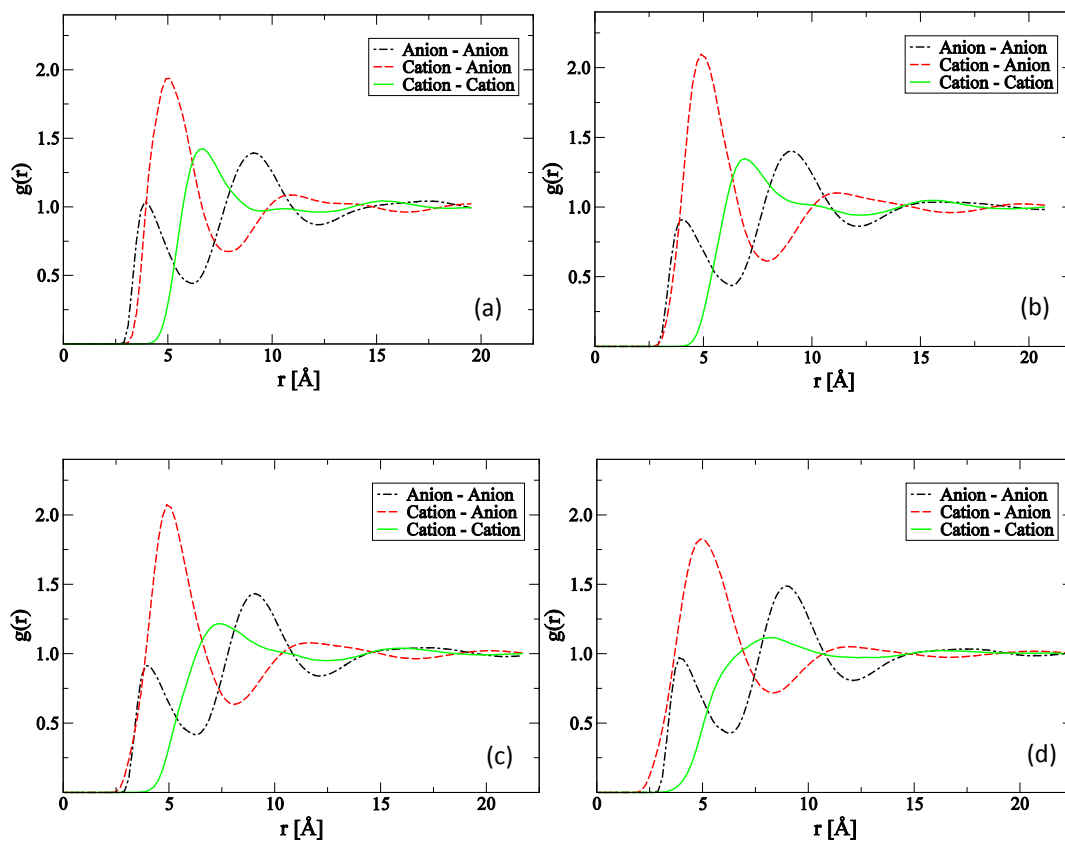
Figure 6: Radial distribution function $g(r)$ for the anion-anion (black), anion-cation (red) and cation-cation (green) center of mass of (a) $[C_2mim^+][TCM^-]$, (b) $[C_4mim^+][TCM^-]$, (c) $[C_6mim^+][TCM^-]$ and (d) $[C_8mim^+][TCM^-]$ at 298.15 K.
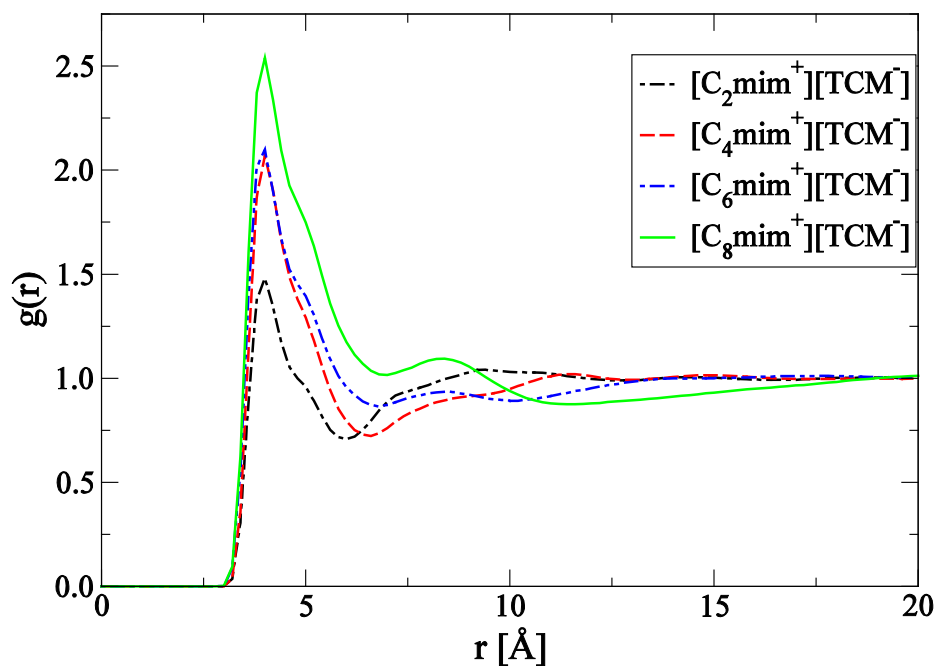
Figure 7: Radial distribution function $g(r)$ between the terminal carbon atoms in the cation alkyl chain of $[C_2mim^+][TCM^-]$ (black), $[C_4mim^+][TCM^-]$ (red), $[C_6mim^+][TCM^-]$ (blue) and $[C_8mim^+][TCM^-]$ (green) at 298.15 K.
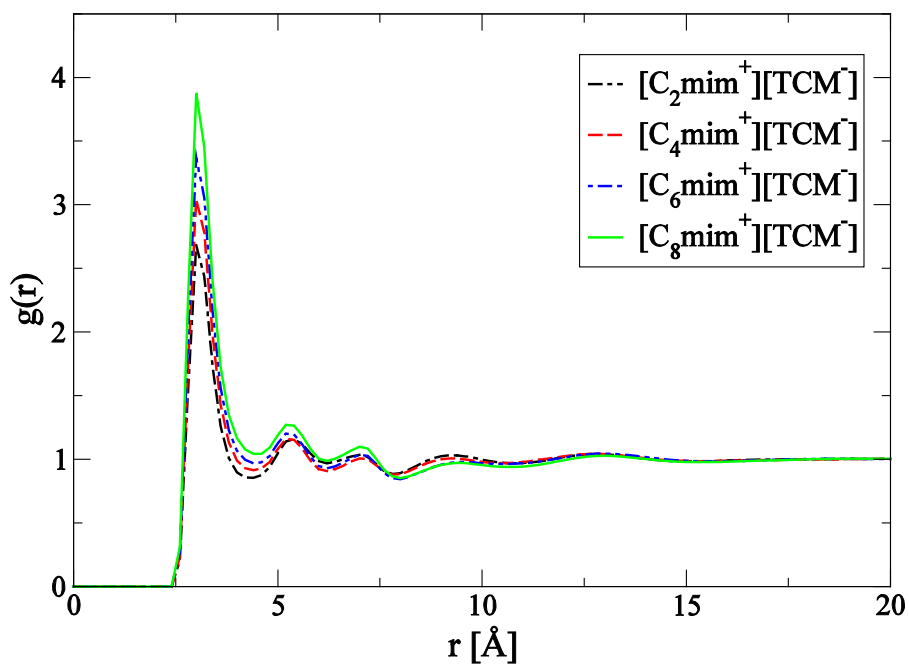
Figure 8: Radial distribution function $g(r)$ between the C2 carbon of the cation imidazolium ring and the NC nitrogen of the anion for [C₂mim⁺][TCM⁻] (black), [C₄mim⁺][TCM⁻] (red), [C₆mim⁺][TCM⁻] (blue) and [C₈mim⁺][TCM⁻] (green) at 298.15 K.
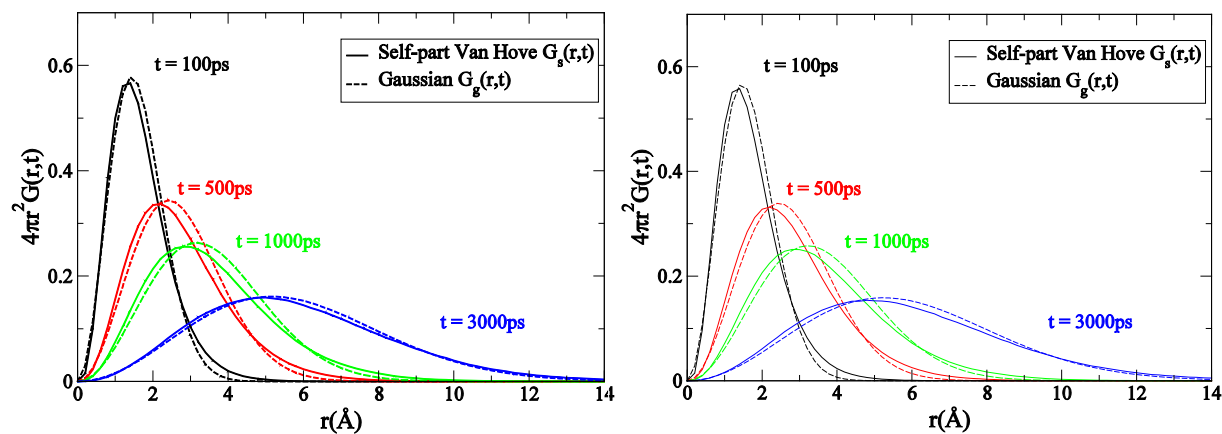
Figure 9: Self-part of the Van Hove function $G_s(r,t)$ at 298.15 K plotted against the expected Gaussian distribution for (a) cation (left) and (b) anion of $[C_4mim^+][TCM]$ (right).
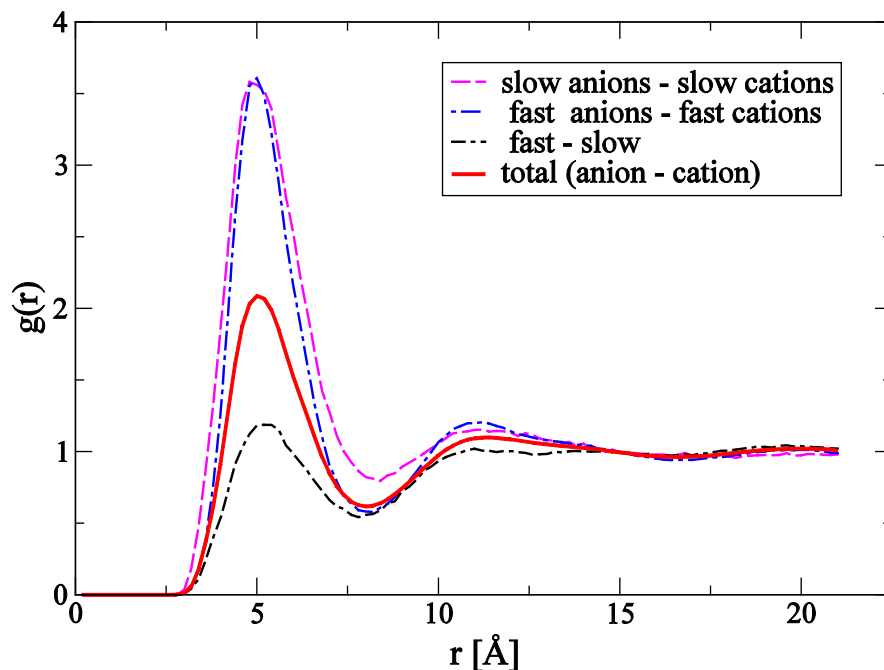
Figure 10: Radial distribution functions between the centers of mass of slow anions – slow cations (magenta), fast anions – fast cations (blue) and fast – slow anions and cations (black) plotted against the total $g(r)$ (red) calculated for [C_4mim^+][TCM^-] at 298.15 K for $t = 500$ ps. The red line corresponds to the radial distribution functions between the anion-cation centers of mass as calculated from all ions.

References

1.   E. J. Maginn, *J. Phys.: Condens. Matter*, 2009, **21**, 373101-373118.
2.   H. Weingärtner, *Angew. Chem. Int. Ed.*, 2008, **47**, 654-670.
3.   K. N. Marsh, J. A. Boxall and R. Lichtenthaler, *Fluid Phase Equilib.*, 2004, **219**, 93-98.
4.   E. W. Castner and J. F. Wishart, *J. Chem. Phys.*, 2010, **132**, 120901.
5.   Q. Dai, D. B. Menzies, D. R. MacFarlane, S. R. Batten, S. Forsyth, L. Spiccia, Y.-B. Cheng and M. Forsyth, *C. R. Chim.*, 2006, **9**, 617-621.
6.   P. Wang, S. M. Zakeeruddin, M. Grätzel, W. Kantlehner, J. Mezger, E. V. Stoyanov and O. Scherr, *Appl. Phys. A*, 2004, **79**, 73-77.
7.   G. W. Meindersma, A. R. Hansmeier and A. B. de Haan, *Ind. Eng. Chem. Res.*, 2010, **49**, 7530-7540.
8.   Y. Kondo, T. Koyama, R. Tsuboi, M. Nakano, K. Miyake and S. Sasaki, *Tribol. Lett.*, 2013, **51**, 243-249.
9.   M. Marszalek, Z. Fei, D.-R. Zhu, R. Scopelliti, P. J. Dyson, S. M. Zakeeruddin and M. Grätzel, *Inorg. Chem.*, 2011, **50**, 11561-11567.
10.   M. Bidikoudi, T. Stergiopoulos, V. Likodimos, G. E. Romanos, M. Francisco, B. Iliev, G. Adamova, T. J. S. Schubert and P. Falaras, *J. Mater. Chem. A*, 2013, **1**, 10474-10486.
11.   P. Wang, B. Wenger, R. Humphry-Baker, J.-E. Moser, J. Teuscher, W. Kantlehner, J. Mezger, E. V. Stoyanov, S. M. Zakeeruddin and M. Grätzel, *J. Am. Chem. Soc.*, 2005, **127**, 6850-6856.
12.   E. H. Cha, S. A. Lim, J. H. Park, D. W. Kim and D. R. Macfarlane, *J. Power Sources*, 2008, **178**, 779-782.
13.   A. I. Labropoulos, G. E. Romanos, E. Kouvelos, P. Falaras, V. Likodimos, M. Francisco, M. C. Kroon, B. Iliev, G. Adamova and T. J. S. Schubert, *J. Phys. Chem. C*, 2013, **117**, 10114-10127.
14.   O. Tzialla, C. Veziri, X. Papatryfon, K. G. Beltsios, A. Labropoulos, B. Iliev, G. Adamova, T. J. S. Schubert, M. C. Kroon, M. Francisco, L. F. Zubeir, G. E. Romanos and G. N. Karanikolos, *J. Phys. Chem. C*, 2013, **117**, 18434-18440.
15.   G. E. Romanos, L. F. Zubeir, V. Likodimos, P. Falaras, M. C. Kroon, B. Iliev, G. Adamova and T. J. S. Schubert, *J. Phys. Chem. B*, 2013, **117**, 12234-12251.
16.   O. Borodin, *J. Phys. Chem. B*, 2009, **113**, 11463-11478.
17.   T. Yan, C. J. Burnham, M. G. Del Popolo and G. A. Voth, *J. Phys. Chem. B*, 2004, **108**, 11877-11881.
18.   O. Borodin and G. D. Smith, *J. Phys. Chem. B*, 2006, **110**, 11481-11490.
19.   C. Schröder, *Phys. Chem. Chem. Phys.*, 2012, **14**, 3089-3102.
20.   C. Schröder and O. Steinhauser, *J. Chem. Phys.*, 2008, **128**, 224503.
21.   F. Dommert, K. Wendler, R. Berger, L. Delle Site and C. Holm, *ChemPhysChem*, 2012, **13**, 1625-1637.
22.   T. I. Morrow and E. J. Maginn, *J. Phys. Chem. B*, 2002, **106**, 12807-12813.
23.   B. L. Bhargava and S. Balasubramanian, *J. Chem. Phys.*, 2007, **127**, 114510.
24.   H. Liu and E. Maginn, *J. Chem. Phys.*, 2011, **135**, 124507.
25.   E. Androulaki, N. Vergadou, J. Ramos and I. G. Economou, *Mol. Phys.*, 2012, **110**, 1139-1152.
26.   N. Sieffert and G. Wipff, *J. Phys. Chem. B*, 2006, **110**, 13076-13085.

27.   W. Zhao, H. Eslami, L. Cavalcanti Welchy and F. Müller-Plathe, *Z. Phys. Chemie*, 2007, **221**, 1647.
28.   T. G. A. Youngs and C. Hardacre, *ChemPhysChem*, 2008, **9**, 1548-1558.
29.   V. Chaban, *Phys. Chem. Chem. Phys.*, 2011, **13**, 16055-16062.
30.   V. V. Chaban and O. V. Prezhdo, *Phys. Chem. Chem. Phys.*, 2011, **13**, 19345-19354.
31.   V. V. Chaban, I. V. Voroshylova and O. N. Kalugin, *Phys. Chem. Chem. Phys.*, 2011, **13**, 7910-7920.
32.   M. Salanne, *Phys. Chem. Chem. Phys.*, 2015, **17**, 14270-14279.
33.   M. L.S. Batista, J. A.P. Coutinho and J. R.B. Gomes, *Curr. Phys. Chem.*, 2014, **4**, 151-172.
34.   G. E. Logotheti, J. Ramos and I. G. Economou, *J. Phys. Chem. B*, 2009, **113**, 7211-7224.
35.   Y. Zhang and E. J. Maginn, *J. Phys. Chem. B*, 2012, **116**, 10036-10048.
36.   D. Roy, N. Patel, S. Conte and M. Maroncelli, *J. Phys. Chem. B*, 2010, **114**, 8410-8424.
37.   M. Bühl, A. Chaumont, R. Schurhammer and G. Wipff, *J. Phys. Chem. B*, 2005, **109**, 18591-18599.
38.   T. Cremer, C. Kolbeck, K. R. J. Lovelock, N. Paape, R. Wölfel, P. S. Schulz, P. Wasserscheid, H. Weber, J. Thar, B. Kirchner, F. Maier and H. P. Steinrück, *Chem.- Eur. J.*, 2010, **16**, 9018-9033.
39.   C. Hardacre, J. D. Holbrey, C. L. Mullan, M. Nieuwenhuyzen, T. G. A. Youngs, D. T. Bowron and S. J. Teat, *Phys. Chem. Chem. Phys.*, 2010, **12**, 1842-1853.
40.   I. Leontyev and A. Stuchebrukhov, *Phys. Chem. Chem. Phys.*, 2011, **13**, 2613-2626.
41.   I. V. Leontyev and A. A. Stuchebrukhov, *J. Chem. Phys.*, 2014, **141**, 014103.
42.   A. Rahman, *Physical Review*, 1964, **136**, A405-A411.
43.   P. A. Hunt, B. Kirchner and T. Welton, *Chem.- Eur. J.*, 2006, **12**, 6762-6775.
44.   S. M. Urahata and M. C. C. Ribeiro, *J. Chem. Phys.*, 2004, **120**, 1855-1863.
45.   C. Schröder, *Bunsenmagazin*, 2012, **6**, 230-234.
46.   C. M. Breneman and K. B. Wiberg, *J. Comp. Chem.*, 1990, **11**, 361-373.
47.   C. Lee, W. Yang and R. G. Parr, *Phys. Rev. B*, 1988, **37**, 785-789.
48.   S. Kossmann, J. Thar, B. Kirchner, P. A. Hunt and T. Welton, *J. Chem. Phys.*, 2006, **124**, 174506.
49.   J. P. Perdew, K. Burke and M. Ernzerhof, *Phys. Rev. Lett.*, 1996, **77**, 3865-3868.
50.   J. N. Canongia Lopes and A. A. H. Pádua, *J. Phys. Chem. B*, 2004, **108**, 16893-16898.
51.   F. Weigend and M. Häser, *Theor. Chem. Acc.*, 1997, **97**, 331-340.
52.   F. Weigend, M. Häser, H. Patzelt and R. Ahlrichs, *Chem. Phys. Lett.*, 1998, **294**, 143-152.
53.   R. Krishnan, J. S. Binkley, R. Seeger and J. A. Pople, *J. Chem. Phys.*, 1980, **72**, 650-654.
54.   F. Weigend and R. Ahlrichs, *Phys. Chem. Chem. Phys.*, 2005, **7**, 3297-3305.
55.   P. Schulz, Institute of Chemical Reaction Engineering, University of Erlangen-Nuremberg, Germany, personal communication.
56.   T. M. Koller, M. H. Rausch, J. Ramos, P. S. Schulz, P. Wasserscheid, I. G. Economou and A. P. Fröba, *J. Phys. Chem. B*, 2013, **117**, 8512-8523.
57.   C. Cadena and E. J. Maginn, *J. Phys. Chem. B*, 2006, **110**, 18026-18039.
58.   M. G. Martin, E. J. Maginn, R. D. Rogers, G. Voth and M. S. Gordon, Technologies for Developing Predictive Atomistic and Coarse-Grained Force Fields for Ionic Liquid Property Prediction, http://handle.dtic.mil/100.2/ADA486185).
59.   M. S. Kelkar, W. Shi and E. J. Maginn, *Ind. Eng. Chem. Res.*, 2008, **47**, 9115-9126.

60. C. Cadena, Q. Zhao, R. Q. Snurr and E. J. Maginn, *J. Phys. Chem. B*, 2006, **110**, 2821-2832.
61. J. C. Phillips, R. Braun, W. Wang, J. Gumbart, E. Tajkhorshid, E. Villa, C. Chipot, R. D. Skeel, L. Kalé and K. Schulten, *J. Comp. Chem.*, 2005, **26**, 1781-1802.
62. P. J. Flory, *Statistical mechanics of chain molecules*, Interscience Publishers, 1969.
63. D. N. Theodorou and U. W. Suter, *Macromolecules*, 1985, **18**, 1467-1478.
64. D. N. Theodorou and U. W. Suter, *Macromolecules*, 1986, **19**, 139-154.
65. P. P. Ewald, *Ann. Phys.*, 1921, **369**, 253-287.
66. M. Tuckerman, B. J. Berne and G. J. Martyna, *J. Chem. Phys.*, 1992, **97**, 1990-2001.
67. G. J. Martyna, M. E. Tuckerman, D. J. Tobias and M. L. Klein, *Mol. Phys.*, 1996, **87**, 1117-1157.
68. M. Królikowski, K. Walczak and U. Domańska, *J. Chem. Thermodyn.*, 2013, **65**, 168-173.
69. M. Larriba, P. Navarro, J. García and F. Rodríguez, *Ind. Eng. Chem. Res.*, 2013, **52**, 2714-2720.
70. R. L. Gardas, M. G. Freire, P. J. Carvalho, I. M. Marrucho, I. M. A. Fonseca, A. G. M. Ferreira and J. A. P. Coutinho, *J. Chem. Eng. Data,* 2007, **52**, 1881-1888.
71. P. J. Carvalho, T. Regueira, L. M. N. B. F. Santos, J. Fernandez and J. A. P. Coutinho, *J. Chem. Eng. Data*, 2010, **55**, 645-652.
72. G. Papavassiliou and M. Fardis, Nuclear Magnetic Resonance Laboratory, Institute of Nanoscience and Nanotechnology, NCSR "Demokritos", Greece - Unpublished results.
73. U. Domańska, M. Królikowska and K. Walczak, *Colloids Surf. A: Physicochem. Eng. Aspects*, 2013, **436**, 504-511.
74. Y. Wang and G. A. Voth, *J. Phys. Chem. B*, 2006, **110**, 18601-18608.
75. A. A. H. Pádua, M. F. Costa Gomes and J. N. A. Canongia Lopes, *Acc. Chem. Res.*, 2007, **40**, 1087-1096.
76. J. N. A. Canongia Lopes and A. A. H. Pádua, *J. Phys. Chem. B*, 2006, **110**, 3330-3335.
77. Y. Wang, W. Jiang, T. Yan and G. A. Voth, *Acc. Chem. Res.*, 2007, **40**, 1193-1199.
78. E. Androulaki, N. Vergadou and I. G. Economou, *Mol. Phys.*, 2014, **112**, 2694-2706.
79. L. Van Hove, *Physical Review*, 1954, **95**, 249-262.
80. W. Kob, C. Donati, S. J. Plimpton, P. H. Poole and S. C. Glotzer, *Phy. Rev. Lett.*, 1997, **79**, 2827-2830.